Available online at www.sciencedirect.com
ScienceDirect
International Journal of Mass Spectrometry 265 (2007) 347–358
International Journal of Mass Spectrometry
www.elsevier.com/locate/ijms

In situ recognition of molecular chirality by mass spectrometry Hydration effects on differential stability of homo- and heterochiral dimethyltartrate clusters

Eugene N. Nikolaev [a,*], Igor A. Popov [a,1], Oleg N. Kharybin [b], Alexey S. Kononikhin [c], Marina I. Nikolaeva [a,1], Yurij V. Borisov [d]

[a] *The Institute for Energy Problems of Chemical Physics, Russian Academy of Sciences, Leninskij pr. 38, k.2, Moscow 117813, Russia*
[b] *The Institute for Biomedical Chemistry, Russian Academy of Medical Sciences, Pogodinskaya str., 10, Moscow 119832, Russia*
[c] *The Institute for Biochemical Physics, Russian Academy of Sciences, Kosygin str. 4, Moscow 119991, Russia*
[d] *A.N. Nesmeyanov Institute of Organoelement Compounds, Russian Academy of Sciences, Vavilov str. 28, Moscow 117813, Russia*

Received 17 November 2006; received in revised form 29 March 2007; accepted 2 April 2007
Available online 29 April 2007

Abstract

We explored a possibility of using atmospheric pressure ionization techniques like corona discharge chemical ionization and surface thermoionization for distinguishing the chiral chemical compounds *in situ*. In both cases of ionization techniques we used home built ion sources coupled with non-modified ThermoFinnigan interfaces. For the proof-of-principle demonstration of recognition of molecule chirality *in situ* we used dimethyltartrate as a model chiral substance. We demonstrated that both ionization methods produce dimers and trimers of the dimethyltartrate molecules with pronounced chiral discrimination effects. In the case of corona discharge ionization we detected H_3O^+ and H_2O^+ based dimers and trimers. K^+ based dimers and trimers dominated the mass spectra in the case of thermoionization. Homochiral domination in the potassiumated dimers and H_2O^+ based dimers can be attributed to inherited chirality effect from the trimers. We showed that addition of the water molecules to dimers strongly influenced the effect of chirality on dimer stability by making heterochiral dimer more stable than homochiral in case of addition of one water molecule and removing the influence of chirality on dimers stability by addition of two or more water molecules. The experimental observations agree well with the results of the quantum chemical calculation obtained for dimers containing different number of water molecules.

Keywords: Recognition of chirality; Atmospheric pressure ionization; Thermoionization

1. Introduction

Feasibility of recognition of the molecular chirality by mass spectrometry has been demonstrated by many groups [1]. In the combination with "kinetic method" [2] it has been applied to solve even some practical problems of controlling chiral purity of drugs [3]. One of the most intriguing and challenging problems for chiral recognition is the detection of the chiral asymmetry in extraterrestrial conditions to answer the question of the origin of homochirality on Earth. There were a lot of discussions about a possibility to detect chiral polarization of molecular sediments on the surface of the Saturn's satellite—Titan [4]. Successful Cassini-Huygens mission to Titan has increased the interest to this subject and further investigations will be undertaken including analyses of the chirality of the organic compounds on its surface. Two other objects of the Solar system: Mars and Europa are considered to be likely to contain organic compounds as well, but to our knowledge there are no nearest plans to investigate their surfaces for the

Abbreviations: DMT, dimethyltartrate; CI, chemical ionization; ESI, electrospray ionization; MALDI, matrix-assisted laser desorbtion/ionization; AP, atmospheric pressure; APCI, atmospheric pressure chemical ionization; CID, collision induced dissociation

* Corresponding author. Tel.: +7 495 1371007; fax: +7 495 1373479.
E-mail addresses: ennikolaev@rambler.ru (E.N. Nikolaev), icrms@yandex.ru (O.N. Kharybin), kononikhin@chph.ras.ru (A.S. Kononikhin), yabor@ineos.ac.ru (Y.V. Borisov).
[1] Tel.: +7 495 1371007; fax: +7 495 1373479.

1387-3806/$ – see front matter © 2007 Elsevier B.V. All rights reserved.
doi:10.1016/j.ijms.2007.04.001

presence of chiral polarization. Harsh conditions on the Titan's surface put strong limitations on the choice of the methodology for *in situ* analyses of the chirality of the organic compounds. Earlier we have already discussed the potential strategies for recognition of chirality of the organic compounds on the Titan's surface [5]. We made a conclusion, that the mass spectrometry is the most adequate technique for this purpose because of its high sensitivity and a possibility for direct identification of the analyzed molecules. Another important practical application of such technique of chiral recognition would be analysis of the chiral purity of the drugs. The possibility of performing analyses under the atmospheric pressure makes this approach especially attractive.

Intrinsically, mass spectrometry provides achiral property of an ion—that is mass to charge ratio. However, the analysis of the molecular chirality becomes possible by analyzing ion–molecular complexes. Homochiral and heterochiral complex usually have different stability. This property allows to distinguish those complexes and to determine their relative abundances. Ion–molecular complexes can be formed by a number of ionization techniques including CI, MALDI and ESI. Those three methods can be used at the near atmospheric pressure, so that only ionized part of the analyte is introduced into the analyzer and they need only low pumping capacity of mass spectrometer vacuum system. Among those three methods, the CI is the most simple and robust. The most simple implementation of CI is atmospheric pressure CI (APCI) caused by corona discharge. It is quite possible to monitor ion–molecular complexes in APCI conditions. For example in water containing atmosphere water clusters $H^+(H_2O)_n$ with n up to 50 dominates mass spectrum at room temperature (see below).

To our knowledge surface thermoionization being one of the oldest and well characterized techniques of positive and negative ion production in high vacuum has never been used as a method of ionization at atmospheric pressure. In this paper we characterized APCI by corona discharge and AP surface thermoionization as methods for *in situ* determination of enantiomeric composition by direct probing of the analyte vapors. As a model substance we used dimethyltartrate. This substance has two chiral centers. It is solid at room temperature and has vapor pressure of about 10^{-6} Torr. It has strong effect of chirality in the formation of protonated dimers and trimers. Also the thermodynamics and kinetics of their cluster formation is well characterized [6–9]. To distinguish between left and right forms of DMT molecules we labeled left form of the DMT by substituting both methyl groups with deuterated ones. It has been shown before that this substitution does not affect the stability of the protonated DMT cluster.

2. Instruments

For the detection of the corona discharge ionization source products we used ThermoFinnigan SSQ 710C single quadrupole and ThermoFinnigan LCQ DECA-XP ion trap mass spectrometers. For detection of the surface thermoionization products we used Only ThermoFinnigan LCQ DECA-XP. In the case of liquid samples it is possible to do both ESI and APCI without modification of the standard ThermoFinnigan ion sources. For API of gas samples we introduce a simple modification by adding a corona discharge needle on one holder and heated wire of NiCr alloy on the other. The corona discharge was ignited by high voltage from the standard API ion source.

2.1. Ionization source

2.1.1. Corona discharge source

The home built corona discharge API source is shown on Fig. 1. It is similar to what was described earlier [10]. The source consists of a tungsten wire tip approximately 10 μm in diameter, producing a discharge in a point-to-plane geometry with the 500 μm i.d. stainless steel heated inlet capillary of the mass spectrometer. The corona discharge is located in a volume between the tip and capillary inlet. The tip-to-capillary distance can be varied and was chosen to support stable corona. Voltages ranging from 2 to 4 kV were applied to the tip using a ThermoFinnigan (formerly Finnigan MAT, San Jose, CA) electrospray ionization power supply through a 1 GΩ (Caddock Electronics, Riverside, CA) resistor placed in series with the tip that acts to limit and stabilize the discharge current. A point-to-plane corona discharge is used to produce primary ions, which ionize the trace organic vapors through a series of ion–molecule reactions. It is well known that in the corona discharge source working in positive ion mode a rapid sequence of ion–molecule reactions occurs to form a series of protonated water molecular clusters of the type $(H_2O)_nH^+$ [11]. Fig. 2 shows a typical example of a mass spectrum of laboratory air. It was measured at room temperature of desolvating capillary using ThermoFinnigan SSQ 710C single quadrupole mass spectrometer. As we can see corona discharge ionization method gives mass spectra, which are sensitive not only to proton affinities in the positive ionization mode and electron affinity in the negative mode, but also sensitive to thermo-chemistry of complex formation. Peak $H^+(H_2O)_{21}$ in water cluster series corresponding to the structure of enhanced stability dominates in the mass spectrum. These protonated clusters are formed in the chain of ion molecular reactions started from N_2^+ and O_2^+ ions, formed in corona discharge, which then were converted into H_2O^+ giving H_3O^+, the last two ions serve

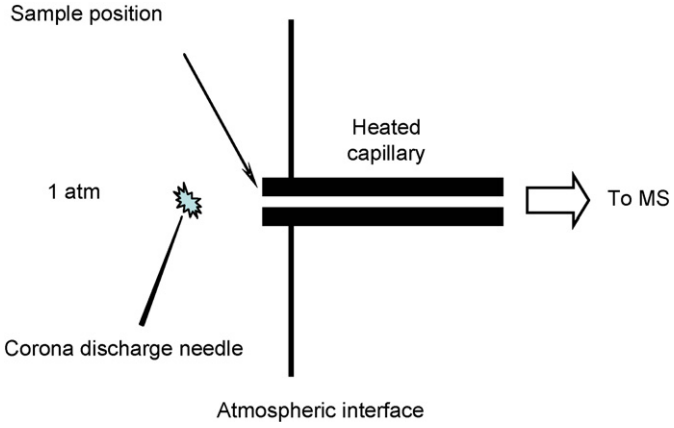

Fig. 1. Corona discharge source setup.

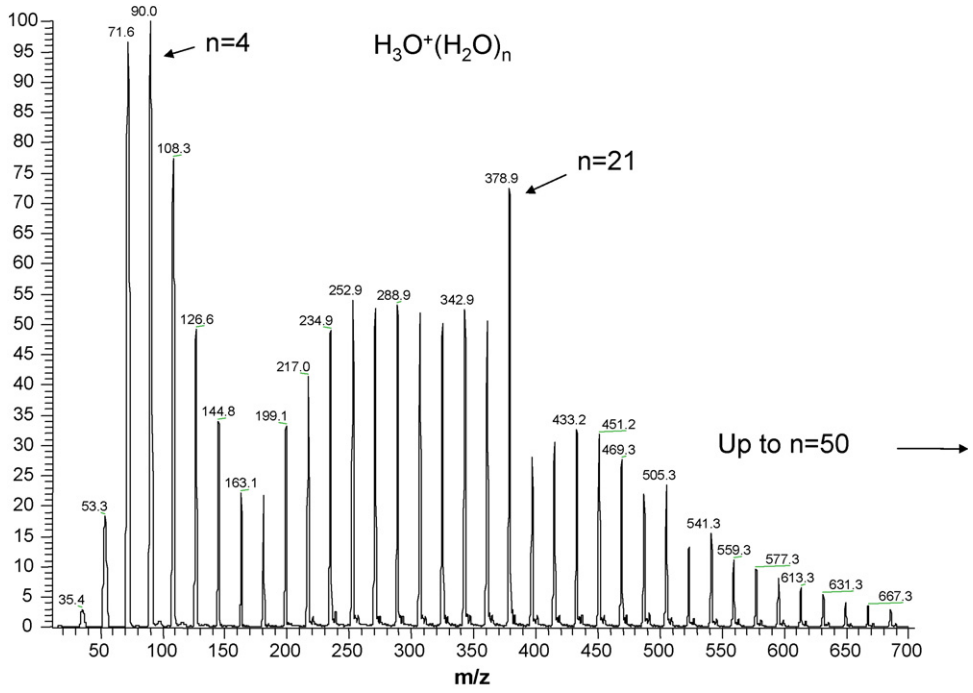

Fig. 2. Corona discharge ionization mass spectrum from air at room temperature.

as a primary reagent ions for ionization of the trace components of the gas mixture. The weakly bound (by hydrogen bonds) clusters can be easily declustered in the heated capillary or by the use of collision induced dissociation (CID) at an intermediate pressure (∼1 Torr). [11,12]. With ThermoFinnigan LCQ DECA we did not see such a long series of water clusters. Usually the number of water molecules in the cluster did not exceed 10.

2.1.2. Thermoionization ion source

The home built AP thermoionization source is shown on Fig. 3. NiCr alloy wire of 0.2 mm in the diameter was used as a surface thermoionization ion source. The wire-to-capillary distance is variable and was chosen to produce maximal signal. The wire was heated by current from Russian made power supply supporting up to 3 A. Current ranging from 1.5 to 2 A was used to produce primary ions, mainly alkali metal cations when redheated, which cationize the analyte vapors (trace organic) through a series of ion–molecule reactions. These cations are captured by an airflow and sucked into the 500 μm i.d. stainless steel heated inlet capillary of the mass spectrometer. Samples with sufficiently high vapor pressure were placed in front of capillary. Nonvolatile samples were placed as a solution or as small crystals directly onto the heating wire. In both cases of ionization (corona and thermoionization) we used manufacturer's non-modified ion optics, which consists of a heated inlet capillary for ions desolvation as they enter the vacuum system, a tube lens for ion focusing at high pressure in to the aperture of a skimmer, followed by an rf-only octopole ion guide. Ions traversing the ion guide pass another aperture and enter the analytical quadrupole or ion trap. Detection of the ion signal is performed using an off-axis conversion dynode/multiplier combination. Instrument control and data acquisition in the case of corona discharge instrument is done by Finnigan ICIS software running on a Digital Unix workstation. In the case of surface ionization experiments we used standard LCQ PC based Windows software.

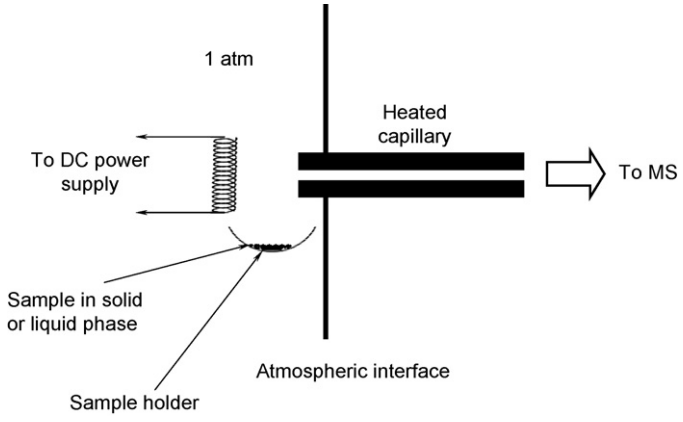

Fig. 3. Thermoionization source setup.

3. Results and discussion

3.1. In situ recognition of DMT chirality in vapor using corona discharge ion source

To recognize the chirality of the vaporized DMT molecules, which penetrate into the corona discharge region we deposited isotopically labeled L-DMT samples on the surface of heated capillary of the ESI source (see Fig. 1). This labeled sample produces protonated monomers, dimers and trimers in API mass

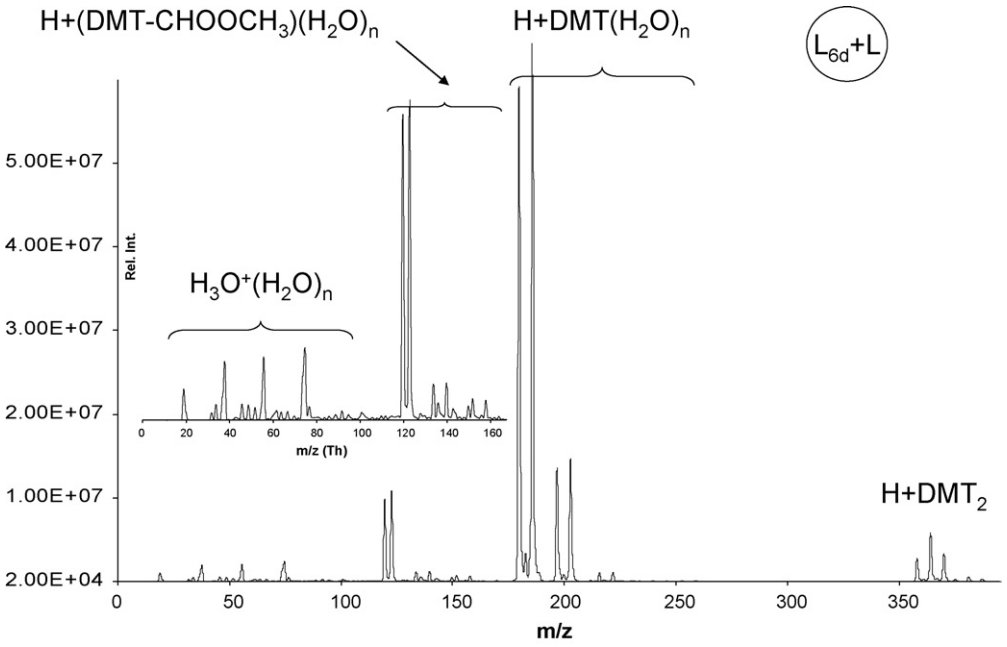

Fig. 4. DMT vapors in laboratory air at 90 °C: L + L_{6d}. Where L is left DMT molecule and L_{6d} is isotopically labeled L-DMT molecule, in which two CH_3 groups are substituted by CD_3 groups (L_{6d} notation is used on following figures as well, for right DMT molecules we are using notation D).

spectra when the temperature of the capillary is higher then 70 °C. At the temperatures around 70 °C the spectra is dominated by hydrated DMT clusters. At the temperatures higher than 100 °C, pure DMT cluster and DMT decomposition products dominate. When non-labeled L-DMT samples are approaching corona region we observe mixed (deuterated and non deuterated) dimers and trimers formation. Fig. 4 shows the part of mass spectrum obtained using corona discharge ionization of non-labeled and labeled DMT molecules mixture measured at 90C. Intensity distribution inside dimer group is statistical (binomial) as it was anticipated in the case of absence of isotopic effect. However, we observe strong discrimination of heterochiral dimers when we introduce D-DMT sample vapors into the corona region (Fig. 5). This behavior has already been observed in CI equilibrium and ESI experiments [13,14]. Because labeled reference DMT sample is positioned directly on the desolvating capillary the relative intensity of the homochiral D-dimers and heterochiral dimers depends on the distance between the sample holder

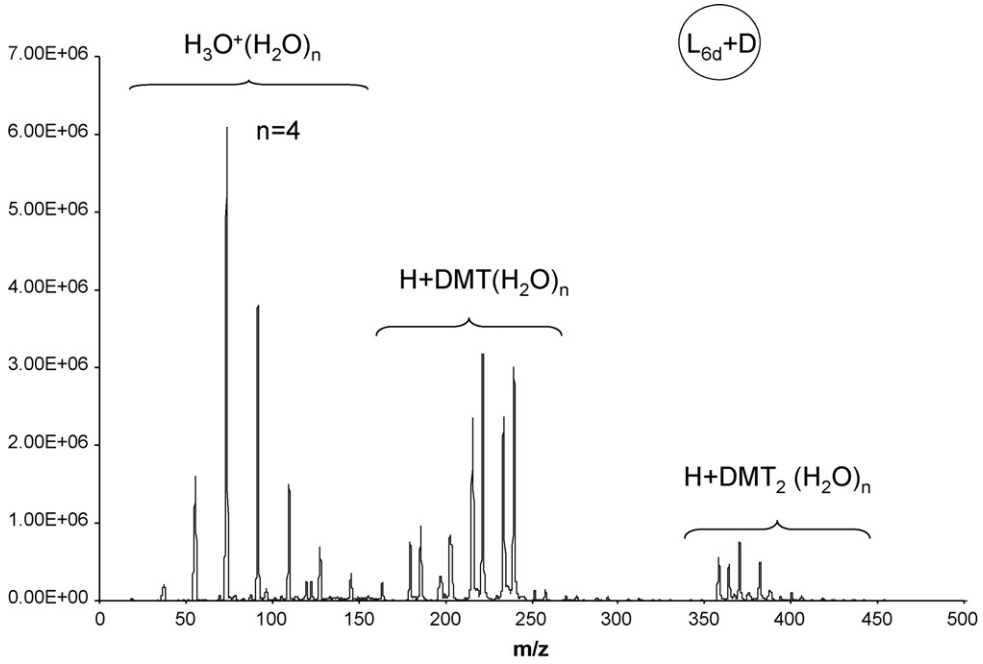

Fig. 5. DMT vapors in laboratory air at 80 °C: D + L_{6d}.

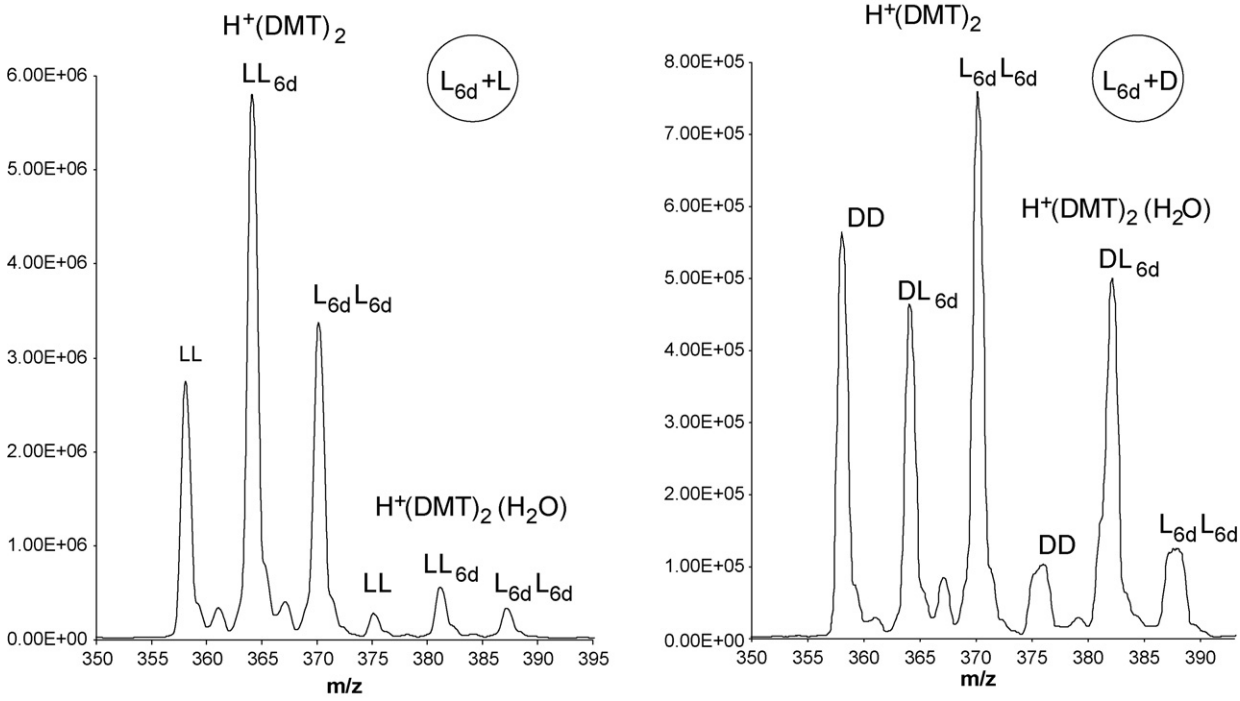

Fig. 6. Protonated DMT dimers from molecules of the same (left) and different (right) chirality.

and the corona discharge region. By adjusting this distance we made the intensities of those dimers comparable. Detectable signal is observed at distance of around 1 cm. In another experiment when both reference (deuterated L-DMT) sample and analyzed sample were positioned in the same sample holder as a mixture of two enantiomers the relative intensities of homochiral L-containing and D-containing dimers were independent of the distance and depended only on the relative concentrations of enantiomers in the mixture. Fig. 6 shows the cases, when the dimers presented as a mixture of the molecules of the same (left) and different chirality (right). In both cases, besides protonated dimers we also observed water containing dimers. As we can see homochiral species were dominated by protonated dimers while the heterochiral species were dominated by hydrated dimers. Heterodimer domination was first observed by Nikolaev and McMahon during studies of ion–molecular reactions in left and right DMT molecules mixture by FT-ICR mass spectrometer with high pressure ion source [15].

As shown on Fig. 7 trimers were presented by both homochiral and heterochiral mixtures. The interference between the protonated and hydrated trimers does not obscure the fact that in the hetero mixture there is a discrimination of homotrimer among the protonated trimers and even stronger discrimination among the hydrated trimers. Occasionally we were observing

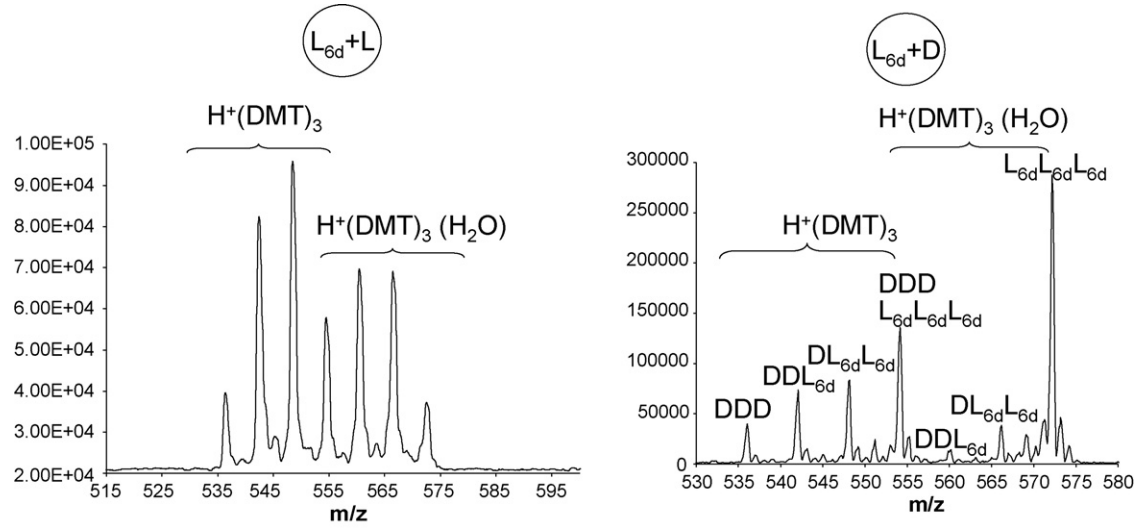

Fig. 7. Protonated DMT trimers from molecules of different chirality.

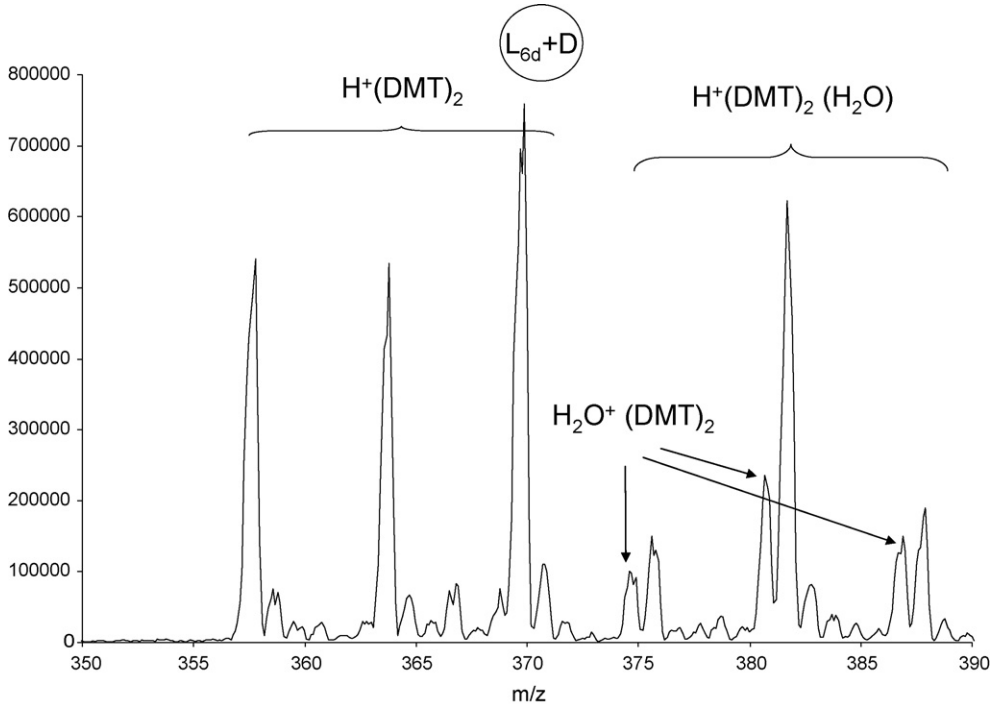

Fig. 8. Protonated DMT dimers from molecules of different chirality: $L_{6d} + D$.

not only protonated dimers and trimers but also H_2O^+ based cluster series. Fig. 8 shows the dimer for hetero mixture of the DMT molecules with $H_2O^+(DMT)_2$ group. It is evident that the intensity distribution for this group is closer to statistical, in contrast to proton containing dimers. Fig. 9 shows the high m/z part of spectrum presented on Fig. 5. We identified a series of $H^+(DMT)_2\ (H_2O)_n$ clusters. The detectable end of this series is shown on Fig. 10. As we can see starting from two water molecules inside the cluster there is no discrimination between homo- and heterochiral clusters. The relative intensities of the dimers follow the binomial distribution.

3.2. In situ recognition of DMT vapor chirality using AP thermoionization ion source

AP thermoionization of laboratory atmosphere air generates both positive and negative ions with the total ion current lower by about one order of magnitude compared to corona discharge ionization. We did not specially treat the surface of heated wire to increase the emission of alkali ions. The observed current originated from the impurities. We observed ions with masses up to 2000 Da in positive mode and up to 4000 Da in negative mode. This observation is difficult to explain and requires further

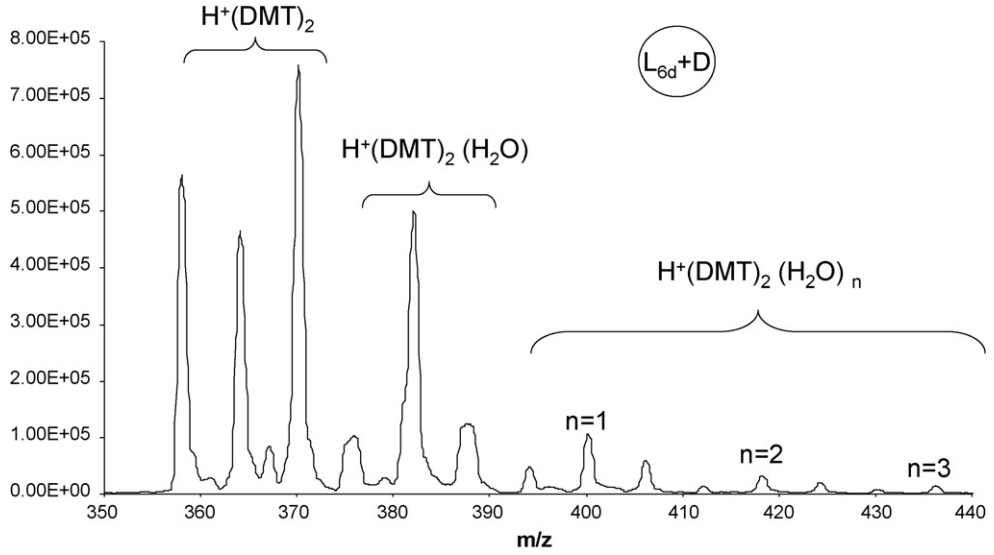

Fig. 9. Water containing protonated dimers $H^+(DMT)_2\ (H_2O)_n$.

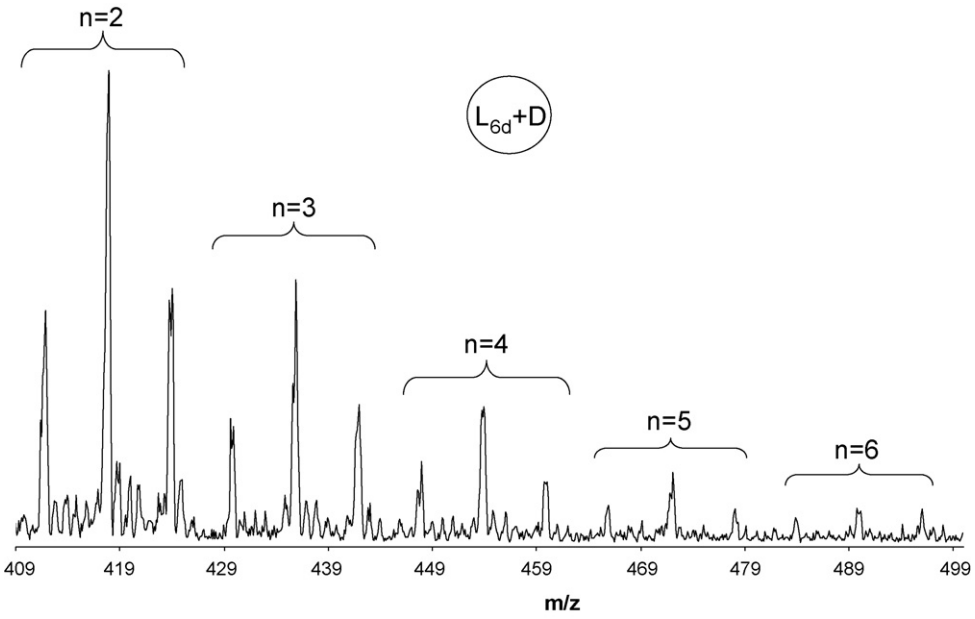

Fig. 10. Water containing protonated dimers $H^+(DMT)_2\ (H_2O)_n$ (higher n).

investigation using a high-resolution mass spectrometer. Fig. 11 shows an example of a positive ions mass spectrum obtained for background air. Signal intensities were highly sensitive to the presence of different organic substances in the atmosphere and on the heated capillary. We tested AP thermoionization at the surface as a method for *in situ* analysis of the enantiomeric composition by direct probing of the analyte vapors. Fig. 12 shows an example of mass spectrum of thermoionization of dimethyltartrate vapors. As in the case of corona discharge experiments to distinguish between left and right forms of DMT molecules we labeled L-form by substituting both methyl groups with deuteriorated methyl group. We found a strong influence of chirality on formation of cation-based dimers and trimers supporting of the results from earlier experiments using CI. In the case of thermoionization we saw only Na^+ and K^+ based dimers and trimers. The extent of chiral discrimination is comparable with what we saw before on the protonated DMT dimers and trimers in case of corona discharge ionization. It is known from ion molecular reaction of ligand exchange equilibrium that chiral discrimination of DMT does not exist in alkali ion-based dimers

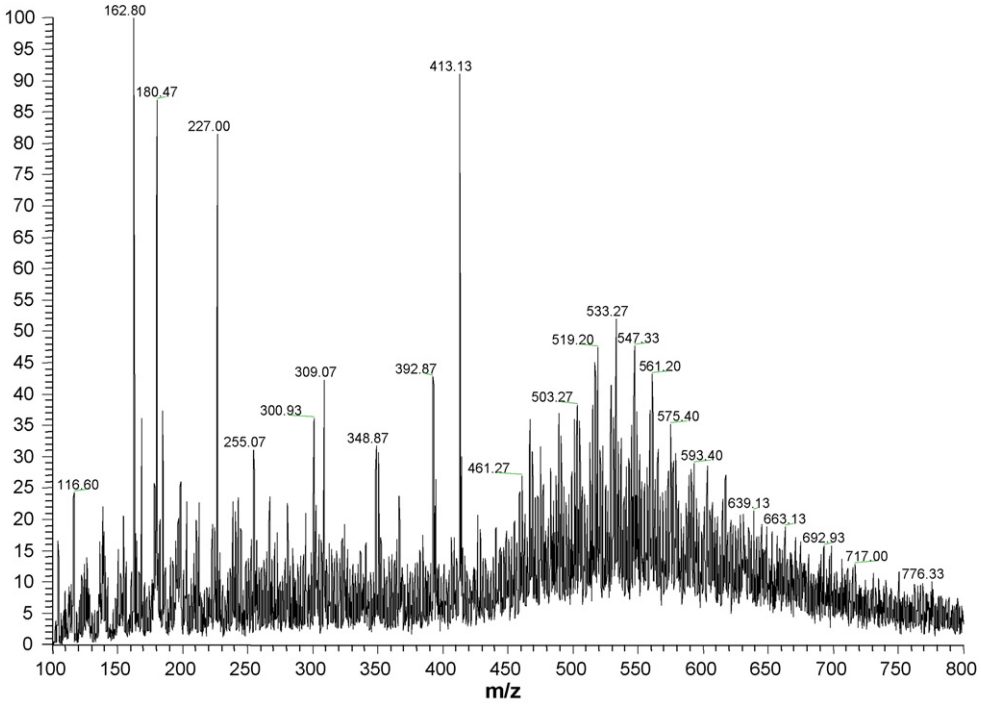

Fig. 11. Atmospheric pressure thermoinization mass spectrum of laboratory air.

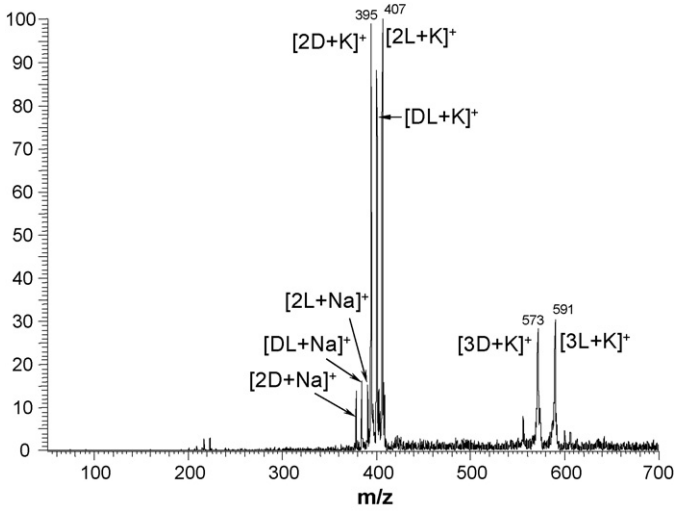

Fig. 12. Atmospheric pressure thermoinization mass spectrum of DMT wapors: $D + L_{6d}$.

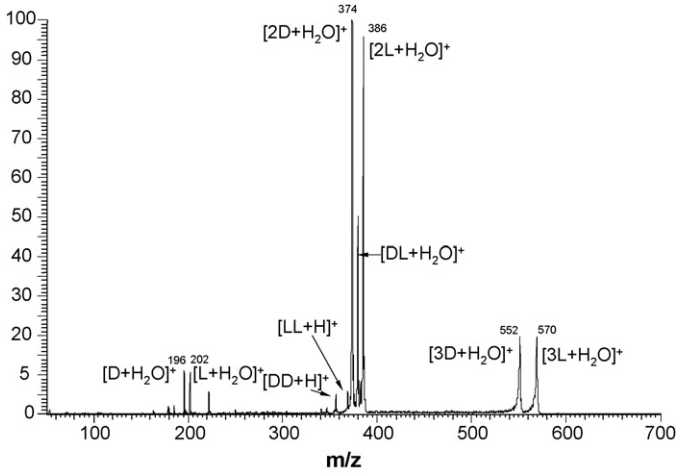

Fig. 13. Atmospheric pressure corona discharge chemical ionization mass spectrum of DMT vapors: $D + L_{6d}$.

[16]. Observed chiral discrimination in alkali ions based dimers can be explained by formation of those dimers from trimers through the dissociation of trimers within the ion transportation system. Homochiral combinations strongly dominate the trimer complexes. After trimer decompositions the dimer products inherit[1] homodomination and showing chirality effect in intensity distribution. We have repeated corona discharge CI using the same setup as in the thermoionization experiments (on LCQ DECA-XP). Using the ion trap we saw only small intensity peaks of protonated dimers in the case of corona discharge ionization (Fig. 13). The intensity distribution inside this peak group demonstrates complete elimination of protonated heterochiral dimer in these conditions. H_2O^+ based dimers and trimers dominated in the spectrum. Within dimer and trimer groups spectra were dominated by the homochiral species. The strong difference in the relative intensities of the peaks, corresponding to protonated and H_2O^+ dimers (Figs. 8 and 13) can be explained by the differences in humidity and DMT vapor concentration. Proton transfer from H_3O^+ to DMT monomers produces protonated DMT monomers, followed by formation of protonated dimers. At low humidity and high DMT partial pressure, the DMT molecules interacting with H_2O^+ before these ions get converted into H_3O^+. This mechanism is supported by the kinetics of changing of relative intensities of H_2O^+ based monomer complexes to H_3O^+ based monomer complexes (Fig. 14). This kinetics was measured when DMT sample was extracted from the reaction region. From our observations it follows that the value of chiral discrimination in the case of H_2O^+ based dimers strongly depends on the experimental conditions. The R ratio of abundances (sum of the intensities of homochiral dimers to intensity of heterochiral) of homochiral to heterochiral dimers is changing from statistical $R = 1$ (absence of chiral discrimination) to up to $R = 3$ (strong chiral discrimination). It is reasonable to suggest that the chirality effect observed for this dimer group has a similar nature to what we saw for alkali metal-based dimer and determined by the inheritance from the trimers. This method of chirality recognition may not be applied to any chemical compound. The compound should be volatile enough to form dimers by APCI and AP thermoionization. Moreover, the chirality must have an affect on the stability of dimers or trimers. A chiral drug albicar is an example of a compound with high enough volatility but no chiral discrimination in the dimer stability. L-albicar was labeled with six deuterium atoms. We saw very intense peaks of albicar dimers both in AP CI and AP thermoionization mass spectra. Figs. 15 and 16 show the comparison of the spectra obtained by corona discharge CI and thermoionization. From these figures it becomes evident that albicar molecules form complexes according to statistical distribution without revealing any significant chirality effects in stability of both dimer and trimer groups.

3.3. Influence of hydration on chiral discrimination in DMT dimer formation

The results on Figs. 9 and 10 showing that attaching more than one water molecule destroys the bonds between the tartrate molecules responsible for chiral discrimination in dimer formation process. It means that in the bulk phase we should not see such discrimination. To investigate this effect further we calculated the potential surface fragments for homo- and heterochiral DMT dimers containing zero, one or two water molecules. All calculations were performed at the density functional B3LYP level of theory [17,18]. Optimized geometry parameters and frequencies of normal vibrational modes for the studied molecular systems were computed using the 6-31 G* atomic basis sets [19]. Single points on the potential energy surface were calculated having regard to the 6-311++

[1] This effect has a kinetic character. In equilibrium, if there is no thermodynamic preference for one of the forms (homo or hetero) dimers intensity has statistical (binomial) distribution. During the formation in ESI process some of them are formed as result of trimer decomposition in ion transport system or inside ICR cell. So if trimer intensity distribution is not statistical dimers will not be as well. If for instance in trimer group homochiral trimers dominate we will have mainly homochiral dimers, because heterochiral dimers could be formed only from heterochiral trimers.

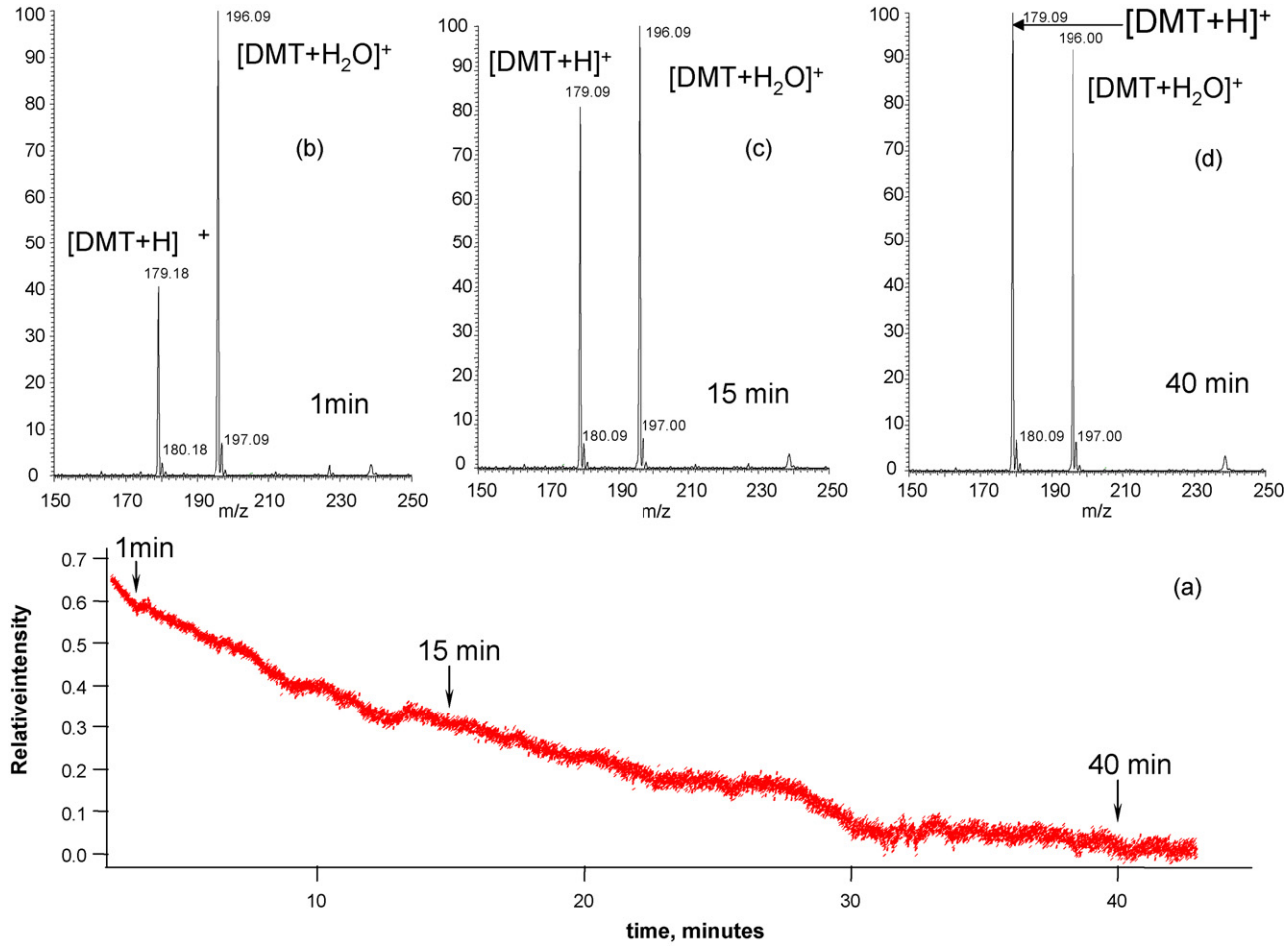

Fig. 14. (a) Kinetics of transformation of H_2O^+ DMT based monomer complexes into H_3O^+ based monomer complexes after removal of DMT sample from corona region, (b) mass spectrum at 1 min, (c) mass spectrum at 15 min, and (d) mass spectrum at 40 min.

G** polarization and diffusion functions [20]. The calculations were performed with the use of the GAUSSIAN-98 program [21] on a CRAY J90 supercomputer in the National Energy Research Supercomputer Center (Oakland, California, USA) and on an SC760-D mini-supercomputer in the A.N. Nesmeyanov Institute of Organoelement Compounds (Moscow, Russian Federation). Calculated values of total (E, a.u.) and relative (ΔE, kcal/mol) energies of LL and LD forms of charged complexes $H^+(DMT)_2(H_2O)_n$ ($n = 0$, 1, 2) for three basis sets 6-31 G*, 6-311 G**,

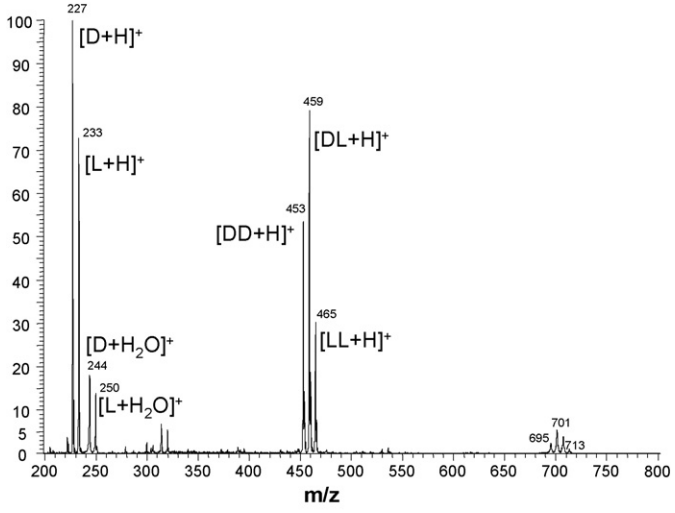

Fig. 15. Atmospheric pressure corona discharge chemical ionization of albicar vapors: D + L_{6d}.

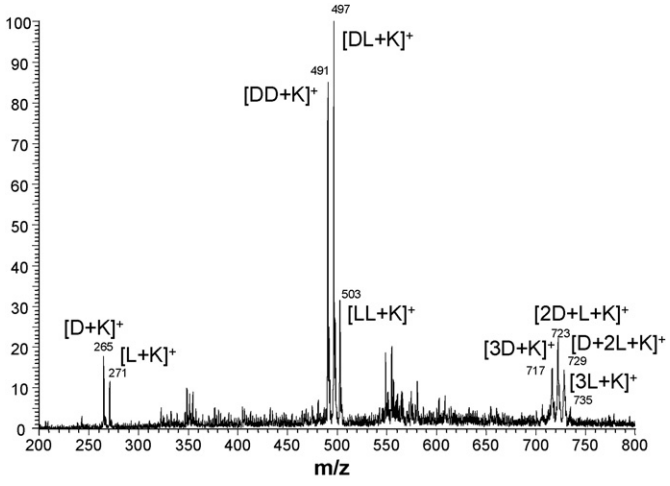

Fig. 16. Atmospheric pressure thermoionization mass spectrum of albicar wapors: D + L_{6d}.

Table 1
Calculated values of total (E, a.u.) and relative (ΔE, kcal/mol) energies of LL and LD forms of charged complexes H^+ $(DMT)_2$ $(H_2O)_n$ ($n = 0, 1, 2$) for three basis sets 6-31 G*, 6-311 G**, 6-311++G**

System	6-31 G*		6-311 G**		6-311++ G**	
	$-E$	ΔE	$-E$	ΔE	$-E$	ΔE
LL H^+ $(DMT)_2$	1372.3636	0.0	1372.7762	0.0	1372.8066	0.0
LD H^+ $(DMT)_2$	1372.3599	2.3	1372.7725	2.3	1372.8033	2.0
LL H^+ $(DMT)_2$ H_2O	1448.7993	4.0	1449.2499	3.6	1449.2834	3.2
LD H^+ $(DMT)_2$ H_2O	1448.8056	0.0	1449.2556	0.0	1449.2886	0.0
LL H^+ $(DMT)_2$ $(H_2O)_2$	1525.2425	0.8	1525.7302	0.6	1525.7657	1.3
LD H^+ $(DMT)_2$ $(H_2O)_2$	1525.2438	0.0	1525.7311	0.0	1525.7677	0.0

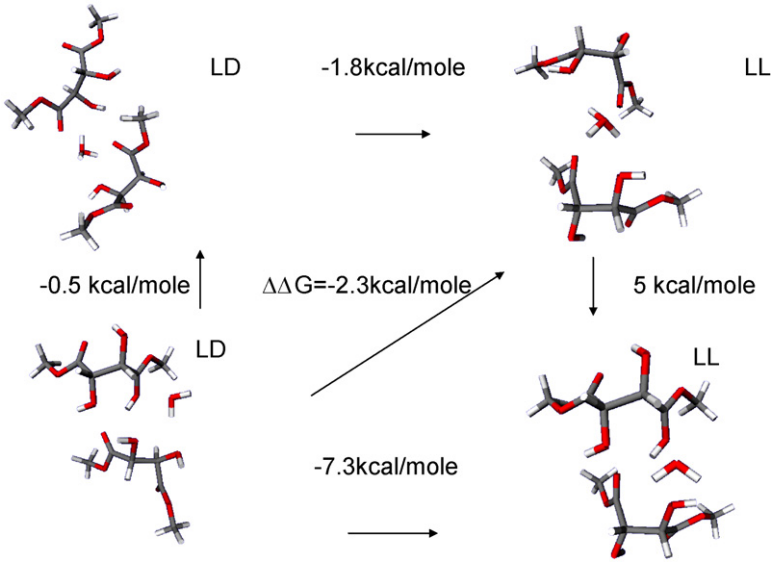

Fig. 17. $H^+(DMT)_2$ (H_2O) group. Ab initio Becke, Lee, Yang, Parr Method in 6-311 G* bases.

6-311++ G** are presented in Table 1. Fig. 17 shows the minimum energy structures and transitions energies for one water molecule containing DMT homo- and heterodimers. In the upper part of the figure we show structures with protonated water molecule. In the lower part we show the structures where proton is located on the DMT molecule and unprotonated water interacting with the DMT molecule through a hydrogen bond. It is evident that configuration of homochiral dimer with protonated water molecule has the lowest energy. The energy of the heterochiral dimer with protonated water molecule is higher by 1.8 kcal/mole. This is in agreement with experimental observations, where homochiral dimer was more stable than heterochiral. For the conformations with protonated DMT molecule the difference in formation energy is much higher—7.3 kcal/mole. Fig. 18 shows the minimum energy structures for tartrates homo- and heterodimers containing two water molecules. It is evident that proton is located on one of the water molecules and the other water molecule forms hydrogen bonds between the DMT molecules. The energy difference indicates that the heterochiral structure is more stable than the homochiral as we observed in the experiments. Table 2 presents the calculated values of hydrogen bond distances (R(O–H)) and charges on H- and O-atoms forming H-bonds (qH, qO) for LL and LD forms of complexes H^+ $(DMT)_2$ $(H_2O)_n$ ($n = 0, 1, 2$) (6-311++ G** basis set). We would like to note, that from the data (Table 2) for all three considered systems $H^+(DMT)_2$ $(H_2O)_n$ ($n = 0, 1, 2$) the transition from LL to LD form is not accompanied by the variation in the number of hydrogen bonds, but only quantitative characteristics of hydrogen bonds. By the quantitative characteristics we mean the lengths of hydrogen bonds and effective charges on atoms of hydrogen and oxygen. For example in more stable LL-form $H^+(DMT)_2$ the length of the shortest hydrogen bond is less, than in the LD-form. The shortest hydrogen bond in the LD-form of the dimer with one molecule

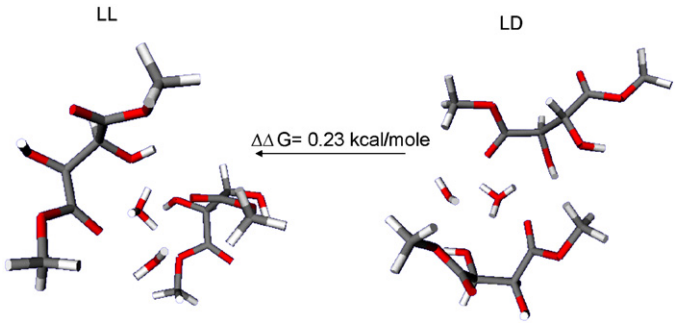

Fig. 18. $H^+(DMT)_2$ $(H_2O)_2$ group. Ab initio Becke, Lee, Yang, Parr Method in 6-311 G* bases.

Table 2
Calculated values of hydrogen bond distances (R(O–H)) and charges on H- and O-atoms forming H-bonds (qH, qO) for LL and LD forms of charged complexes $H^+(DMT)_2(H_2O)_n$ ($n = 0, 1, 2$) (6-311++ G** basis set)

System	R(O–H)	qH	qO
LL $H^+(DMT)_2$	H(17)–O(30) = 1.7206	0.4951	−0.2345
	H(18)–O(24) = 2.4144	0.4359	−0.2637
LD $H^+(DMT)_2$	H(17)–O(30) = 1.7328	0.5270	−0.2258
	H(23)–O(24) = 2.0430	0.4644	−0.2491
LL $H^+(DMT)_2 H_2O$	H(23)–O(1) = 1.5889	0.2724	−0.2936
	H(47)–O(9) = 1.6416	0.4438	−0.2880
	H(48)–O(24) = 1.6046	0.4628	−0.3472
LD $H^+(DMT)_2 H_2O$	H(23)–O(24) = 1.5256	0.4023	−0.2971
	H(47)–O(9) = 1.6679	0.4598	−0.2487
	H(48)–O(30) = 1.7253	0.3229	−0.1561
LL $H^+(DMT)_2 (H_2O)_2$	H(48)–O(32) = 1.6297	0.4555	−0.2003
	H(23)–O(49) = 1.4533	0.3256	−0.4592
	H(50)–O(24) = 1.9880	0.2534	−0.3342
	H(51)–O(1) = 1.8701	0.4015	−0.2938
	H(47)–O(9) = 1.5740	0.3803	−0.2329
LD $H^+(DMT)_2 (H_2O)_2$	H(48)–O(30) = 1.7230	0.3970	−0.1543
	H(23)–O(49) = 1.5194	0.3829	−0.4376
	H(50)–O(10) = 2.0150	0.2580	−0.1488
	H(51)–O(24) = 2.1137	0.3172	−0.3736
	H(47)–O(1) = 1.6763	0.4311	−0.3107

of water is equal to 1.52 and, which is less than in the LL-form (1.59 Å). Analyses of the structure of dimers containing two water molecules shows that the water molecules interact with the DMT molecules in such a way that their chirality do not affect the dimer stability.

4. Conclusions

Using simple experimental setup we demonstrated a possibility of chiral analyses of a mixture of enantiomeres by direct probing the vapors of analyte at the atmospheric pressure conditions. A couple of atmospheric pressure ionization techniques were tested as potential methods for *in situ* recognition of molecular chirality at the atmospheric pressure, such as corona discharge chemical ionization and surface thermoionization. We showed that both methods produce dimers and trimers of dimethyltartrate molecules with pronounced effects of chiral discrimination. In the case of corona discharge ionization we detected both H_3O^+ and H_2O^+ based dimers and trimers of the DMT molecules. K^+ based dimers and trimers dominate the mass spectra produced by the thermoionization technique. We observed homochiral domination in potassiumated dimers and H_2O^+ based dimers and attributed this fact to inherited chirality effect from the trimers. We also showed that addition of water molecules to dimers strongly influences on the effect of chirality on dimer stability making heterochiral dimer more stable than homochiral in the case of addition of one water molecule and removing the influence of chirality on dimers stability by addition of more than one water molecules. Results of the quantum chemical calculation for dimers containing different number of water molecules agree well with the experimental data. They explain the observed effect of dimer hydration on the stability difference between homo- and heterodimers by redistribution of hydrogen bonds between water and DMT molecules.

Acknowledgements

The authors thank Dr. Vladislav Petyuk for his help with preparation of this article. The generous financial support by the Russian Foundation for Basic Research (RFBR grants 05-03-32870, 07-02-01482, 02-02-17131, 06-03-33033), INTAS (grant 05-1000004-7759), Presidium of Russian Academy of Science, Russian Ministry of Education and Science.

References

[1] M. Sawada, Mass Spectrom. Rev. 16 (1997) 73.
[2] W.A. Tao, D. Zhang, E.N. Nikolaev, R.G. Cooks, J. Am. Chem. Soc. 122 (2000) 10598.
[3] L. Wu, R.G. Cooks, Anal. Chem. 75 (2003) 678.
[4] J.I. Lunine, J. Beauchamp, M.A. Smith, E.N. Nikolaev, Adv. Biochirality 1 (1999) 257.
[5] E.N. Nikolaev, V.A. Davankov, J.I. Lunine, W.A. Tao, R.G. Cooks, Adv. Mass Spectrom. 15 (2001) 509.
[6] J.P. Honovich, G.V. Karatchevtsev, E.N. Nikolaev, Rapid Commun. Mass Spectrom. 6 (1992) 429.
[7] E.V. Denisov, V. Shustryakov, E.N. Nikolaev, F.J. Winkler, R. Medina, Int. J. Mass Spectrom. Ion Processes 167/168 (1997) 259.
[8] R.G. Kostyanovsky, E.N. Nikolaev, O.N. Kharybin, G.K. Kadorkina, V.R. Kostyanovsky, Mendeleev Commun. 3 (2003) 97.
[9] A.N. Vilkov, E.V. Denisov, E.N. Nikolaev, Russ. J. Chem. Phys. 19 (8) (2000) 53.
[10] E.N. Nikolaev, L.S. Riter, B.C. Laughlin, E. Handberg, R.G. Cooks, Eur. J. Mass Spectrom. 10 (2) (2004) 197.
[11] W.M. Brubaker, Adv. Mass Spectrom. 4 (1968) 293.
[12] H. Kambara, I. Kanomata, Int. J. Mass Spectrom. Ion Phys. 25 (1977) 129.

[13] E.N. Nikolaev, G.T. Goginashvili, R.G. Kostjanovskij, V.L. Tal'roze, Int. J. Mass Spectrom. Ion Proc. 86 (1988) 249.
[14] E.N. Nikolaev, E.V. Denisov, V.S. Rakov, J.H. Futrell, Int. J. Mass Spectrom. 182/183 (1999) 357.
[15] E.N. Nikolaev, T.B. McMahon, Proceedings of the 43rd ASMS Conference, Atlanta, 1995, p. 973.
[16] E.N. Nikolaev, E.V. Denisov, V.S. Rakov, J.H. Futrell, Adv. Mass Spectrom. 14 (1998) 358.
[17] A.D. Becke, J. Chem. Phys. 98 (1993) 5648.
[18] C. Lee, W. Yang, R.G. Parr, Phys. Rev. B 37 (1988) 785.
[19] M.J. Frish, J.A. Pople, J.S. Binkley, J. Chem. Phys. 80 (1984) 3265.
[20] T.H. Dunning Jr., P.J. Hay, in: H.F. Schaefer III (Ed.), Methods of Electronic Structure Theory, Plenum Press, New York, 1977, p. 1.
[21] M.J. Frisch, G.W. Trucks, H.B. Schlegel, G.E. Scuseria, M.A. Robb, J.R. Cheeseman, V.G. Zakrzewski, J.A. Montgomery Jr., R.E. Stratmann, J.C. Burant, S. Dapprich, J.M. Millam, A.D. Daniels, K.N. Kudin, M.C. Strain, O. Farkas, J. Tomasi, V. Barone, M. Cossi, R. Cammi, B. Mennucci, C. Pomelli, C. Adamo, S. Clifford, J. Ochterski, G.A. Petersson, P.Y. Ayala, Q. Cui, K. Morokuma, D.K. Malick, A.D. Rabuck, K. Raghavachari, J.B. Foresman, J. Cioslowski, J.V. Ortiz, B.B. Stefanov, G. Liu, A. Liashenko, P. Piskorz, I. Komaromi, R. Gomperts, R.L. Martin, D.J. Fox, T. Keith, M.A. Al-Laham, C.Y. Peng, A. Nanayakkara, M. Challacombe, P.M.W. Gill, B. Johnson, W. Chen, M.W. Wong, J.L. Andres, C. Gonzalez, M. Head-Gordon, E.S. Replogle, J.A. Pople, Gaussian 98, Revision A.5, Gaussian Inc., Pittsburgh, PA, 1998.